Neurobiology of Disease

Apoptosis-Inducing Factor Substitutes for Caspase Executioners in NMDA-Triggered Excitotoxic Neuronal Death

Hongmin Wang,[1,2]* Seong-Woon Yu,[1,2]* David W. Koh,[1,2] Jasmine Lew,[1,2] Carmen Coombs,[1,2] William Bowers,[5] Howard J. Federoff,[5] Guy G. Poirier,[6] Ted M. Dawson,[1,2,3] and Valina L. Dawson[1,2,3,4]

[1]Institute for Cell Engineering and Departments of [2]Neurology, [3]Neuroscience, and [4]Physiology, Johns Hopkins University School of Medicine, Baltimore, Maryland 21205, [5]Department of Neurology, Center for Aging and Developmental Biology, University of Rochester, Rochester, New York 14642, and [6]Health and Environment Unit, Laval University Medical Research Center, Centre Hospitalier Universitaire de Québec, Ste-Foy, Quebec G1V 4G2, Canada

The profound neuroprotection observed in poly(ADP-ribose) polymerase-1 (PARP-1) null mice to ischemic and excitotoxic injury positions PARP-1 as a major mediator of neuronal cell death. We report here that apoptosis-inducing factor (AIF) mediates PARP-1-dependent glutamate excitotoxicity in a caspase-independent manner after translocation from the mitochondria to the nucleus. In primary murine cortical cultures, neurotoxic NMDA exposure triggers AIF translocation, mitochondrial membrane depolarization, and phosphatidyl serine exposure on the cell surface, which precedes cytochrome *c* release and caspase activation. NMDA neurotoxicity is not affected by broad-spectrum caspase inhibitors, but it is prevented by Bcl-2 overexpression and a neutralizing antibody to AIF. These results link PARP-1 activation with AIF translocation in NMDA-triggered excitotoxic neuronal death and provide a paradigm in which AIF can substitute for caspase executioners.

Key words: **apoptosis-inducing factor; NMDA; neuronal death; PARP-1; excitotoxicity; nNOS**

Introduction

Glutamate excitotoxicity is thought to play a prominent role in a variety of neurologic disorders (Dawson and Dawson, 1998; Lynch and Guttmann, 2002). NMDA receptor stimulation accounts for the majority of glutamate excitotoxicity with a lesser role for non-NMDA receptor activation (Sattler and Tymianski, 2001). Accompanying the increase in intracellular calcium is the activation of calcium-dependent enzymes and mitochondrial production of reactive oxygen species, which initiate the death of neurons (Sattler and Tymianski, 2001). Activation of neuronal nitric oxide (NO) synthase (nNOS) plays a major role in glutamate excitotoxicity, because pharmacologic inhibition or gene deletion of nNOS results in resistance to a variety of neurologic insults including stroke (Huang et al., 1994; Panahian et al., 1996; Samdani et al., 1997), intrastriatal injections of NMDA (Ayata et al., 1997), and 1-methyl-4-phenyl-1,2,3,6-tetrahydropyridine (MPTP) intoxication (Przedborski et al., 1996). NO mediates a majority of its toxic effects by reacting with superoxide anion to form peroxynitrite, a potent oxidant (Koppenol et al., 1992). Peroxynitrite can trigger neuronal death by DNA damage and activation of the DNA damage-sensing enzyme poly(ADP-ribose) polymerase-1 (PARP-1) (de Murcia et al., 1994). PARP-1 activation in response to toxic insults has been implicated in cell death in stroke (Eliasson et al., 1997; Endres et al., 1997), MPTP intoxication (Mandir et al., 1999), myocardial infarction (Pieper et al., 2000), streptozozin-induced diabetes (Burkart et al., 1999; Masutani et al., 1999; Pieper et al., 1999), and NMDA excitotoxicity (Mandir et al., 2000), because mice lacking the gene for PARP-1 are dramatically resistant to these toxic insults. PARP-1 activation may kill cells through energy depletion that occurs as a result of the consumption of nicotinamide-adenine dinucleotide (NAD) and ATP (Szabo and Dawson, 1998; Ha and Snyder, 1999) or through PARP-1-dependent release of apoptosis-inducing factor (AIF) (Yu et al., 2002; Du et al., 2003).

The mitochondrial-associated protein AIF is a caspase-independent death-effector molecule (Susin et al., 1999; Daugas et al., 2000). When AIF is released from the mitochondria, it translocates to the nucleus to initiate high molecular weight DNA fragmentation, chromatin condensation, and cell death, independent of caspase activity (Susin et al., 1999; Daugas et al., 2000). PARP-1 activation is required for AIF translocation during cell death initiated by NMDA excitotoxicity (Yu et al., 2002), and AIF plays a significant role in PARP-1-mediated cell death induced by *N*-methyl-*N*′-nitro-*N*-nitrosoguanidine (MNNG)

Received May 8, 2004; revised Oct. 19, 2004; accepted Oct. 24, 2004.

This work was supported by grants from the National Institutes of Health (NS39148), the Robert Packard Center for ALS Research at Johns Hopkins Medical Institutions, the American Heart Association, and the Mary Lou McIlhaney Scholar Award. T.M.D. is the Leonard and Madlyn Abramson Professor in Neurodegenerative Diseases. Under an agreement between the Johns Hopkins University and Guilford Pharmaceuticals, T.M.D. and V.L.D. are entitled to a share of sales royalty received by the university from Guilford. The terms of this arrangement are being managed by the university in accordance with its conflict-of-interest policies.

*H.W. and S.-W.Y. contributed equally to this work.

Correspondence should be addressed to Dr. Valina L. Dawson, Institute for Cell Engineering, Department of Neurology, Johns Hopkins University School of Medicine, 733 North Broadway Street, Suite 731, Baltimore, MD 21205. E-mail: vdawson@jhmi.edu.

DOI:10.1523/JNEUROSCI.3461-04.2004

 0270-6474/04/2410963-11$15.00/0

(Yu et al., 2002). AIF translocation occurs after toxic insults including trauma, cerebral ischemia, hypoxia–ischemia, and MPTP toxicity (Zhang et al., 1994; Yu et al., 2002; Ferrer and Planas, 2003; Zhu et al., 2003). Because glutamate excitotoxicity appears to involve mechanisms that are primarily independent of caspase activation, we further explored the potential role of AIF in glutamate excitotoxicity and examined the relationship of AIF release to PARP-1 activation and indices of apoptosis. Here, we show that AIF appears to translocate to the nucleus before cytochrome *c* (Cyt C) release and caspase activation after NMDA receptor activation. Furthermore, NMDA-glutamate receptor-mediated excitotoxicity occurs through PARP-1-mediated AIF release in a caspase-independent manner.

Materials and Methods

Primary cortical cultures. Primary cortical cell cultures were prepared from gestational day 16 fetal mice. Briefly, the cortex was dissected, and the cells were dissociated by trituration in modified Eagle's medium (MEM), 20% horse serum, 25 mM glucose, and 2 mM L-glutamine after a 25 min digestion in 0.027% trypsin–saline solution (Invitrogen, San Diego, CA). The neurons were plated on 24-well plates coated with polyornithine or on chambered cover glass (Fisher Scientific, Houston, TX) coated with polyornithine and mouse laminin (Sigma, St. Louis, MO). The cultures were inhibited with 5-fluoro-2′-deoxyuridine for 3 d to inhibit proliferation of non-neuronal cells. Neurons were maintained in MEM, 10% horse serum, 25 mM glucose, and 2 mM L-glutamine in an 8% CO_2 humidified 37°C incubator. The growth medium was refreshed twice per week. In mature cultures, neurons represent 70–90% of the total number of cells. Neurons [14 d *in vitro* (DIV)] were exposed to NMDA as described previously (Gonzalez-Zulueta et al., 1998). Cells were washed with control salt solution (CSS) [containing (in mM): 120 NaCl, 5.4 KCl, 1.8 $CaCl_2$, 25 Tris-Cl, 15 glucose, pH 7.4], exposed to 500 μM NMDA plus 10 μM glycine in CSS for 5 min, and were then postexposed in MEM, 21 mM glucose for various time before fixation, immunocytochemical staining, and confocal laser scanning microscopy.

Immunocytochemistry and confocal microscopy. Primary cortical neurons were washed twice with ice-cold Tris-buffered saline (TBS) before fixation with ice-cold methanol. After blocking with 4% normal goat serum in TBS, cells were incubated with the primary antibody (Ab) against AIF or Cyt C (6H2.B4; PharMingen, San Diego, CA) for 4 hr. Cells were washed with blocking solution three times and incubated with the secondary antibody conjugated with fluorescein-5-isothiocyanate (FITC) or Cy3 (PharMingen) for 1 hr. Nuclei were stained with Toto-3 to assess nuclear morphology (1 μM) (Molecular Probes, Eugene, OR) for 10 min after secondary antibody incubation and two rinses with TBS. Exposure of phosphatidyl serine and mitochondrial membrane potential were monitored in live cells with FITC-conjugated annexin-V (100 ng/ml; R&D Systems, Minneapolis, MN) or tetramethyrhodamine methyl ester (TMRM) (100 nM; Molecular Probes), respectively. Confocal microscopy was performed on a LSM510 laser-scanning microscope (Zeiss, Oberkochen, Germany) equipped with an argon laser and two HeNe lasers. Images were obtained by scanning stained cells under 40× oil objectives. Neurons showing nuclear staining of AIF were scored as positive for AIF translocation. When cells lost the punctate Cyt C or TMRM-staining patterns or showed a diffused pattern, they were counted as positive for the release of Cyt C or depolarization of the mitochondrial membrane potential. Nuclei were considered shrunken when the size of nucleus was ≤50% of control nuclei size. A clear cytoplasmic membrane staining was determined as positive for annexin-V staining. For each sample, at least 10 different regions were scanned, and over 200 cells were examined for each data point in at least three independent experiments. In separate assays, viability was determined by computer-assisted cell counting after staining of all nuclei with 1 μg/ml Hoescht 33342 (Molecular Probes) and dead cell nuclei with 7 μM propidium iodide (Sigma) (Mandir et al., 2000).

Intrastriatal NMDA injection. PARP-1 and wild-type mice were maintained on a congenic 129 Sv/Ev background. Male mice (22–28 gm) were used. Stereotactic microinjection of NMDA was performed as described previously (Mandir et al., 2000). The animals were anesthetized with 45 mg/kg pentobarbital via intraperitoneal injection. Bilateral burr holes were made, and NMDA was injected into the right striatum using the following coordinates: rostral, −0.7 mm; lateral, −2.0 mm; and ventral, −4.0 mm from bregma, and an equal volume of PBS was injected in the left striatum using the following coordinates: rostral, −0.7 mm; lateral, −2.0 mm; and ventral, −4.0 mm from bregma. Injection of NMDA (66.7 mM in 0.3 μl) or vehicle (PBS) was made over 10 min, and the needle was left in place for an additional 8 min after injection. Mice were analyzed 6 hr after injection.

Brain sectioning and immunohistochemical staining. The whole brain was rapidly removed. After rinsing with ice-cold CSS, the brain was imbedded in 4% premelted low melting point agarose (~35°C) (Sigma) in CSS and then immediately placed on ice for gelling. Once the gelling was complete on ice, the imbedded brains were subjected to serial coronal sectioning (50–60 μm in thickness) in 4–10°C CSS via an oscillating tissue slicer (Electron Microscopy Sciences, Fort Washington, PA). Brain slices were fixed with ice-cold methanol, rinsed with TBS, and blocked with normal goat serum before incubation with the AIF and NeuN (neuronal-specific nuclear protein) antibody (1:100 dilution; Chemicon International, Temecula, CA) for 4 hr. The slices were then incubated with the secondary antibody for 45 min and Toto-3 for 10 min before being subjected to confocal microscopy. For each coronal section, only the striatal area was scanned and analyzed. Several sections from at least three wild-type and three PARP-1 knock-out (KO) mice were analyzed.

Brain cell fractionation. The striata were collected and placed in ice-cold homogenation buffer (250 mM sucrose, 10 mM HEPES, 1 mg/ml BSA, 0.5 mM EDTA, and 0.5 mM EGTA, pH 7.4). Striata were homogenized using a hand-held Teflon glass homogenizer (2 ml) by eight strokes and centrifuged at 2000 × *g* for 3 min. Pellet (P1) and supernatant (S1) were separately processed further to fractionate nuclei and mitochondria, respectively. For the nuclear fraction, P1 was resuspended in 1 ml of homogenation buffer and homogenized again. After mixing with 4 ml of sucrose buffer II (2 M sucrose, 5 mM Mg-acetate, 0.1 mM EDTA, 10 mM Tris-HCl, pH 8.0), the solution was layered on top of 4.4 ml of sucrose buffer II and ultracentrifuged at 30,000 × *g* for 45 min. The supernatant was decanted by vacuum aspiration, and the nuclei pellet was recovered from the bottom of the tube by resuspending in sucrose buffer I [containing (in mM): 320 sucrose, 3 $CaCl_2$, 2 Mg-acetate, 0.1 EDTA, 10 Tris-HCl, pH 8.0]. For the mitochondrial fraction, S1 was centrifuged at 12,000 × *g* for 8 min. The pellet was washed with sucrose buffer I and centrifuged at 12,000 × *g* for 10 min. The final mitochondria fraction was resuspended in sucrose buffer I. Nuclear and mitochondria fractions were subjected to Western blot analysis, as above.

Subcellular fractionation. For the fractionation of the cortical neurons, the neurons were washed with ice-cold PBS, resuspended in hypotonic homogenation buffer [containing (in mM): 10 KCl, 1.5 $MgCl_2$, 1 Na-EDTA, 1 Na-EGTA, 1 dithiothreitol, 0.1 PMSF, and 10 Tris-HCl, pH 7.4] containing proteinase inhibitor mixture (Roche, Basel, Switzerland), and left on ice for 30 min. NP-40 (0.1%) was added, and the neurons were homogenized with 40 strokes. The nuclear fraction was obtained by centrifugation at 720 × *g* for 5 min. The supernatant was subjected to centrifugation at 10,000 × *g* for 10 min for the mitochondria fraction. The nuclear fraction was washed twice with the isotonic homogenization buffer (0.25 M sucrose in hypotonic buffer).

Antibodies. The antibodies for AIF and manganese superoxide dismutase (MnSOD) have been described previously (http://www.sciencemag.org/cgi/content/full/297/5579/259/DC1) (Yu et al., 2002). The antibody for PAR is polyclonal antibody 96-10 to poly(ADP-ribose), and it has been described previously (Affar et al., 1998, 1999). Anti-mouse Bcl-2 antibody was obtained from USBiological (Swampscott, MA). NeuN antibody was obtained from Chemicon International, and Cyt C (6H2.B4) antibody was obtained from PharMingen.

Western blotting. Cell lysates or subcellular fractions were size separated through denaturing SDS-PAGE. An equal amount of protein for each sample was heated at 100°C for 5 min with an equivalent volume of sample buffer (containing 4% SDS and 10% β-mercaptoethanol) and loaded onto polyacrylamide gels. The proteins were electrotransferred to

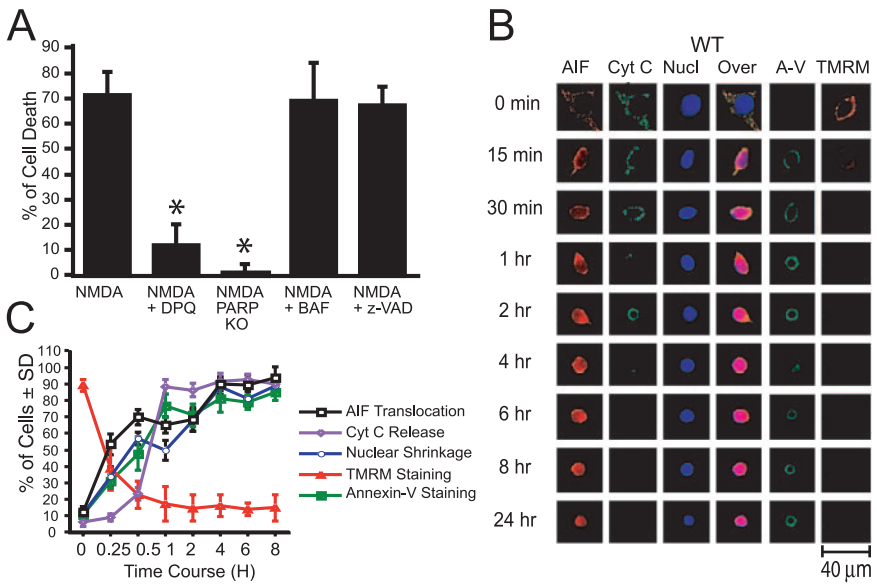

Figure 1. NMDA excitotoxicity is caspase independent, and NMDA induces PARP-1-dependent translocation of AIF. *A*, The effect of PARP-1 or caspase inhibitors on NMDA-induced neuronal cell death. Data are shown for cell death induced by NMDA (500 μM) in the PARP-1 KO cultures or after treatment with the specific PARP inhibitor DPQ (30 μM) or pan-caspase inhibitors z-VAD.fmk (100 μM) or BAF (100 μM) in wild-type (WT) cultures. Data are the mean values of three independent experiments ± SD. Significance was determined by a one-way ANOVA with Student's *t* test; $*p < 0.05$. Representative confocal images (*B*) and quantitative analysis (*C*) of apoptotic events in wild-type cortical cultures exposed to NMDA (500 μM). For each data point, at least 10 different regions were scanned, and over 200 cells were examined in at least three independent experiments. The overlay (Over) represents the fusion image of red (AIF), green (Cyt C), and blue [nucleus (Nucl)] fluorescence. The yellow color reflects the colocalization of AIF and Cyt C in the mitochondrial compartment of the cell. The nucleus turns pink as AIF redistributes into the nucleus. Note the rapid staining of annexin-V (A-V; green) and loss of mitochondrial membrane potential (represented by the loss of red fluorescence of TMRM).These experiments were repeated at least three times with similar results.

a nitrocellulose membrane in Tris–glycine–methanol buffer. The membrane was blocked for 1 hr at room temperature in a blocking solution mixture of 5% nonfat dry milk, 0.05% Tween 20, and TBS, pH 8.0. The membrane was then incubated for 1 hr at room temperature with primary antibody in blocking solution. All primary antibodies are previously characterized antibodies. The membrane was rinsed with blocking solution for five washes of 5 min and incubated for 1 hr at room temperature in peroxidase-labeled secondary antibody. The blot was washed five times for 5 min and then processed for analysis using a Supersignal ChemiLuminiscence detection kit (Pierce, Rockford, IL) as described by the manufacturer.

Fluorogenic caspase-3 assay. Caspase-3-like activity was measured with the ApoAlert Caspase Fluorescent Assay kit (Clontech, Palo Alto, CA) using the provided protocol. Briefly, NMDA-treated neurons were harvested at indicated times in ice-cold PBS. After lysis of an equal number of cells, the lysates were incubated in a 96-well plate with the fluorescent substrate DEVD-AFC (Asp-Glu-Val-Asp-amino-4-trifluoromethyl coumarin). The cleaved free AFC was measured using a fluorescence multiwell plate reader (SOSTmax, Sunnyvale, CA) with an excitation at 400 nm and emission at 505 nm.

Comet assay. Comet assays were conducted by following the protocols provided (Trevigen, Gaithersburg, MD). Briefly, control or NMDA-treated neurons were washed with ice-cold PBS and harvested by centrifugation at 720 × *g* for 10 min. After resuspending at 1×10^5 cells/ml in ice-cold PBS (Ca^{2+} and Mg^{2+} free), the cells were combined with 1% low melting point agarose in PBS (42°C) in a ratio of 1:10 (v/v), and then 75 μl of the cell–agarose mixture was immediately pipetted onto the CometSlide. The sample was then placed flat at 4°C in the dark for 40 min to enhance the attachment. After being lysed in lysis buffer, the sample was washed with 1× Tris borate EDTA buffer and then was transferred and electrophoresed in a horizontal electrophoresis apparatus. The sample was fixed with ethanol and stained with SYBR Green. To quantitatively analyze the length of "comet tails," for each sample, at least 6–10 pictures were taken, and over 600 cells were measured. The comet tail length of each cell was termed as the length from the edge of the nucleus to the end of the comet tail.

Viral transfection. Twenty-four hours before NMDA treatment, neuronal cultures were transduced with either Bcl-2-expressing HSVBcl-2 or β-galactosidase (LacZ)-expressing HSVlacZ herpes simplex viruses [multiplicity of infection (MOI), 100], prepared using a helper virus-free packaging method (Bowers et al., 2001). Under these conditions, >95% of the cells express Bcl-2 or β-galactosidase with minimal toxicity. After 24 hr of infection, the cells were treated with 500 μM NMDA for 5 min and then incubated in MEM containing 21 mM glucose for various times until they were fixed with methanol and stained for AIF and nuclei (Toto-3 staining). Stained cells were scanned with a Zeiss laser confocal microscope and quantitatively analyzed as described above.

Labeling AIF antibody with a fluorescent marker. Labeling the anti-AIF Ab with an amine-reactive probe, FITC (Molecular Probes), was based on the instruction of the company. Briefly, while vortexing 2 mg of Ab (in 0.5 ml, pH >8.0), 50 μl of FITC (dissolved in DMSO, 10 μg/μl) was slowly added into the Ab solution. The reaction was performed for 1 hr at room temperature with stirring, and then the mixture was dialyzed in 20% sucrose overnight at 4°C.

BioPORTER protein delivery system. Antibodies were diluted to 100 μg/ml in PBS (20 mM sodium phosphate, 150 mM NaCl, pH 7.4). The diluted protein solution was added to the dried BioPORTER (Gene Therapy Systems, San Diego, CA) reagent and allowed to rest at room temperature for 5 min followed by gentle mixing. Serum-free medium was added to bring the BioPORTER–protein complex up to 250–300 μl. After washing once in serum-free media, the cell cultures were incubated with the BioPORTER–protein complex for 3–4 hr at 37°C. Cultures were subsequently used for experiments.

Results

AIF release occurs before Cyt C release in NMDA excitotoxicity

Primary cortical neuronal cultures were used to study glutamate excitotoxicity (Fig. 1). NMDA (500 μM) was administered for 5 min to elicit delayed neuronal cell death, as assessed 24 hr later. As reported previously (Eliasson et al., 1997; Yu et al., 2002), under these conditions, NMDA elicits ~60–80% neuronal cell death that is blocked by the potent and selective PARP inhibitor 3,4-dihydro-5-[4-(1-piperidinyl)butoxy]-1(2H)-isoquinolinone (DPQ) (30 μM), and it is completely prevented in cortical neuronal cultures from mice lacking the gene for PARP-1 (Fig. 1*A*). Moreover, the broad-spectrum caspase inhibitors boc-aspartyl-fmk (BAF) (100 μM) and *N*-benzyloxycarbonyl-Val-Ala-Asp-fluoromethyl ketone (z-VAD.fmk) (100 μM) fail to block NMDA excitotoxicity (Fig. 1*A*). Cell death was quantified by cell counting using an objective automated cell-counting system (Gonzalez-Zulueta et al., 1998).

Because NMDA excitotoxicity is PARP-1 dependent and caspase independent, and PARP-1 activation is required for AIF translocation after NMDA receptor stimulation (Yu et al., 2002), we explored the temporal profile of AIF translocation, indices of apoptosis, and markers of PARP-1 activation after NMDA receptor activation. The release of AIF from the mitochondria and its

translocation to the nucleus, nuclear condensation, and phosphatidyl serine exposure on the cell surface as assessed by FITC-conjugated annexin-V staining were monitored over time (see Figs. 1*B*,*C*, 3*C*). In addition, the release of Cyt C and mitochondrial membrane depolarization via TMRM immunofluorescence were examined (see Figs. 1*B*,*C*, 3*C*). However, we cannot exclude the possibility that the decrement in the TMRM may be the result of either mitochondrial depolarization or plasma membrane depolarization resulting from the use of a nonquench mode. Confocal microscopy was used to examine these indices. Representative high-power images are shown in Figure 1*B*, and quantification of these indices are shown in Figure 1*C*. Subcellular fractionations were performed in parallel for AIF nuclear translocation and Cyt C release from the mitochondria (see Fig. 3*C*). A 5 min application of NMDA (500 μM) initiates AIF release from the mitochondria and translocation to the nucleus within 15 min (Fig. 1*B*), as indicated by the appearance of AIF in the nucleus as determined by confocal analysis. Biochemical subcellular fractionation assessment at 30 min after a 5 min application of NMDA also clearly indicates that AIF has translocated to the nucleus (see Fig. 3*C*). AIF continues to translocate to the nucleus after the initial NMDA challenge and appears to be complete within 2 hr in the majority of neurons (Fig. 1*B*,*C*). Accompanying the release and translocation of AIF is marked nuclear condensation, which parallels the time course of AIF translocation (Fig. 1*B*,*C*). Confocal image and Z-plane analysis indicates that the translocation of AIF is not caused by nuclear shrinkage, because AIF is clearly in the nucleus at early time points when the nucleus is clearly distinguishable from cytoplasmic structures (Fig. 1*B*, 15, 30 min, and 1 hr). Annexin-V staining and mitochondrial membrane depolarization also appear to closely parallel AIF translocation (Fig. 1*B*,*C*). z-VAD.fmk at concentrations that completely block the activation of caspase-3 (see Fig. 4) fails to prevent NMDA-induced AIF translocation (see Fig. 3*C*). Cyt C release appears to lag behind AIF translocation and the other indices, because Cyt C immunoreactivity dissipates after AIF translocation (Fig. 1*B*,*C*). Measurable Cyt C release is only detectable after AIF is released from the mitochondria. Biochemical subcellular fractionation assessment of Cyt C release indicates that Cyt C is barely detectable at 1 hr after a 5 min application of NMDA and clearly detectable 2 hr after NMDA administration. Under the methods used, we cannot exclude the possibility that Cyt C is being released at undetectable levels. In contrast, PARP-1 knock-out cortical neurons after NMDA treatment maintain a punctate immunostaining pattern for AIF and Cyt C (Fig. 2*A*,*B*). In addition, mitochondrial membrane potential is not reduced, annexin-V staining is not observed (Fig. 2*A*,*B*), and the nucleus remains undisturbed in PARP-1 KO neurons or wild-type neurons treated with the PARP inhibitor DPQ (Fig. 2*C*). Representative images are shown in Figure 2*C*. Quantification of these results confirm our confocal image analysis (Fig. 2*B*). To further confirm the results of the confocal microscopic analysis that PARP-1 is required for AIF translocation, we evaluated NMDA-treated neuronal cultures by immunoblot assay and subcellular fractionation (Fig. 3*C*). Only the nuclear fractions from wild-type cultures treated with NMDA showed robust AIF bands, but not the nuclear fractions of PARP-1 KO neurons treated with NMDA. Together, these results suggest that NMDA-induced cell death and the translocation of AIF from the mitochondria to the nucleus, as well as the appearance of cell-death markers, are mediated by PARP-1 activation and that AIF release may precede Cyt C release.

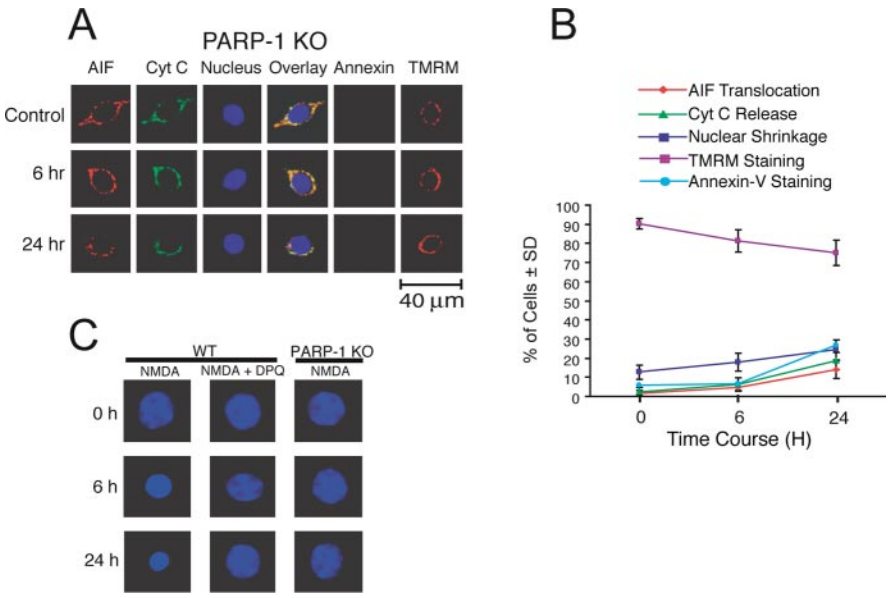

Figure 2. PARP-1 KO cortical cultures are resistant to NMDA treatment. Representative confocal images (*A*) and quantitative analysis (*B*) of apoptotic events in PARP-1 KO cortical cultures exposed to NMDA (500 μM). For each data point, at least 10 different regions were scanned, and >200 cells were examined in at least three independent experiments. PARP-1 KO cultures retain AIF and Cyt C in the mitochondria without annexin-V staining or loss of mitochondrial membrane potential. These experiments were repeated at least three times with similar results. *C*, Confocal analysis of nuclear morphology after NMDA (500 μM) treatment. Nuclear condensation is observed in wild-type (WT) cultures but not in PARP-1 KO cultures or wild-type cultures treated with the specific PARP inhibitor DPQ (30 μM). Scale bar, 5 μm. These experiments were repeated at least three times with similar results.

Temporal profile of AMPA excitotoxicity is different from NMDA excitotoxicity

Previously, we showed that the non-NMDA agonist AMPA causes glutamate excitotoxicity through PARP-1-independent mechanisms (Mandir et al., 2000). To confirm the specificity of the dependence of AIF release on PARP-1 activation after NMDA receptor stimulation, we monitored AIF and Cyt C release via confocal analysis and subcellular fractionation, as well as nuclear shrinkage via confocal analysis after administration of AMPA (Fig. 3). We used conditions that we have shown previously elicit equivalent neuronal cell death (~60–80%) for 500 μM NMDA and 25 μM AMPA (Gonzalez-Zulueta et al., 1998; Mandir et al., 1999). A 5 min application of 25 μM AMPA fails to elicit AIF translocation in both wild-type and PARP-1 KO cortical neurons up to 24 hr later (Fig. 3*A–C*). In contrast, Cyt C is released at ~6–12 hr after AMPA receptor stimulation in wild-type cultures and is released within 6–12 hr in PARP-1 KO cultures. Nuclear condensation is a late event in wild-type cultures, because it is not observed until 24 hr after AMPA administration, whereas in PARP-1 KO cultures, the nucleus begins to condense at 6 hr after AMPA administration (Fig. 3*A*,*B*). These results suggest that AMPA receptor-mediated excitotoxicity occurs through PARP-1- and AIF-independent mechanisms and indicates that the release of Cyt C can be disassociated from the release of AIF. Furthermore, it provides specificity for the role of PARP-1 activation and AIF release in NMDA-mediated excitotoxicity.

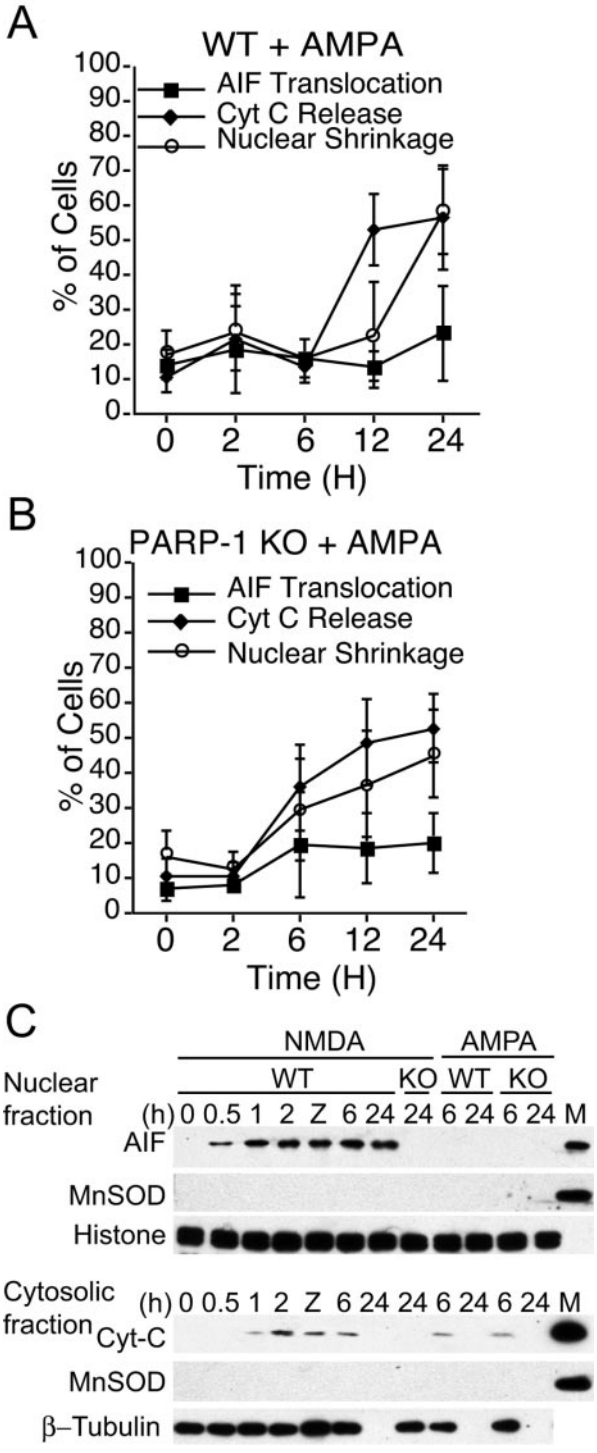

Figure 3. AMPA excitotoxicity fails to induce translocation of AIF. Wild-type (WT; *A*) and PARP-1 KO (*B*) cortical cultures are equally sensitive to AMPA (25 μM) excitotoxicity. Cyt C release and nuclear condensation occur concomitantly, whereas AIF does not translocate during AMPA excitotoxicity. Data are the mean values of three independent experiments ± SD. *C*, Subcellular fractionations of the cortical neurons show that AIF translocates to the nuclei in NMDA-treated wild-type neurons but not in PARP-1 KO neurons. Cyt C translocation to the cytosol appears to occur after AIF translocation after NMDA treatment. AMPA fails to induce AIF translocation in both wild-type and PARP-1 KO neurons, but Cyt C is released into the cytosol, as shown in *A* and *B*. z-VAD.fmk (Z; 100 μM) fails to prevent AIF translocation but shows partial inhibition of Cyt-C release after NMDA treatment in wild-type cultures. Nuclear and cytosolic fractions were subjected to Western blot analysis. Mitochondrial (M) fraction of the untreated wild-type neurons. MnSOD and histone were used as the mitochondrial and nuclear fraction markers, respectively. These experiments were repeated at least three times with similar results.

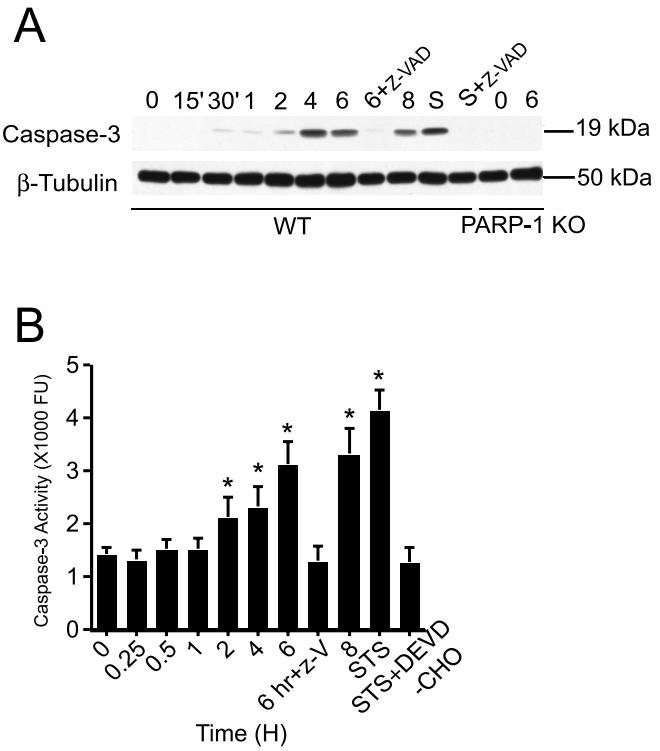

Figure 4. Caspase activation occurs after AIF translocation and nuclear condensation. *A*, In wild-type (WT), but not PARP-1 KO, cortical cultures, exposure to NMDA (500 μM) results in the cleavage of caspase-3 revealed by immunoblot for the activated cleavage fragment. The pan-caspase inhibitor z-VAD.fmk (100 μM) prevents cleavage of pro-caspase-3. Wild-type cortical cultures were treated with 0.5 μM of staurosporine (S) for 8 hr as a positive control for activation of caspase-3. β-Tubulin is a loading control. These experiments were repeated at least two times with similar results. *B*, Time course of caspase activity monitored by cleavage of the fluorescent substrate by measuring the production of free AFC after NMDA (500 μM for 5 min) treatment. z-VAD.fmk blocks caspase activity induced by either NMDA or staurosporine (STS). These experiments were performed at least three times with similar results. Data are the mean values of three independent experiments ± SD. Significance was determined by a one-way ANOVA with Student's *t* test; $^*p < 0.05$.

Caspase-3 activation follows both AIF translocation and nuclear condensation

Because AIF release appears to precede Cyt C release, we examined the relationship between AIF translocation and caspase activation after NMDA excitotoxicity (Fig. 4). Activation of caspase-3 was monitored by an antibody that detects the activated form of caspase-3. Caspase-3 activation is barely detectable 30 min after NMDA glutamate receptor stimulation (Fig. 4*A*), consistent with the observation that Cyt C immunoreactivity begins to decline from cortical neurons at 30 min (Fig. 1*B*,*C*). More significant levels of activated caspase-3 are detected at 2 and 4 hr (Fig. 4*A*,*B*), consistent with the marked dissipation of Cyt C from cortical neurons (Fig. 1*B*,*C*) and the detection of Cyt C in the cytosol via immunoblot analysis (Fig. 3*C*). z-VAD.fmk at concentrations that do not block PARP-1-dependent cell death (Fig. 1*A*) or AIF translocation (Fig. 3*C*) completely blocks the activation of caspase-3 (Fig. 4). The specificity of caspase activation assays was monitored by examining the effects of staurosporine (Fig. 4*A*). Staurosporine (0.5 μM) induces robust caspase-3 activation, as monitored by Western blot analysis (Fig. 4*A*, lane S). z-VAD.fmk completely blocks the activation of caspase-3 induced by staurosporine (Fig. 4*A*). Caspase-3 activity was also detected by the cleavage of a fluorescent caspase-3 substrate

(Miller et al., 1997) (Fig. 4*B*). Activation of caspase-3 activity parallels the appearance of the active fragments, as detected by Western blot analysis at 2, 4, and 6 hr (Fig. 4*A*). Similar to the Western blot analysis of caspase-3 activity, z-VAD.fmk completely prevents caspase-3 activity (Fig. 4*B*) at doses that fail to block NMDA excitotoxicity (Fig. 1*A*) and AIF translocation (Fig. 3*C*). Staurosporine administration confirms the specificity of the caspase activation assay, because it induces robust caspase-3 activity that is blocked by the caspase-3 inhibitor DEVD-CHO (acetyl-aspartyl-glutamyl-valyl-aspart-1-aldehyde) (Fig. 4*B*). Thus, under the conditions used here, the time course of caspase activation parallels the release of Cyt C, consistent with the notion that Cyt C release, and subsequent caspase activation, is a late event in NMDA excitotoxicity, which occurs after AIF translocation. Together, these results suggest that NMDA receptor stimulation causes AIF translocation in a caspase-independent manner and that caspase activation after NMDA receptor stimulation may be a secondary event in NMDA excitotoxicity.

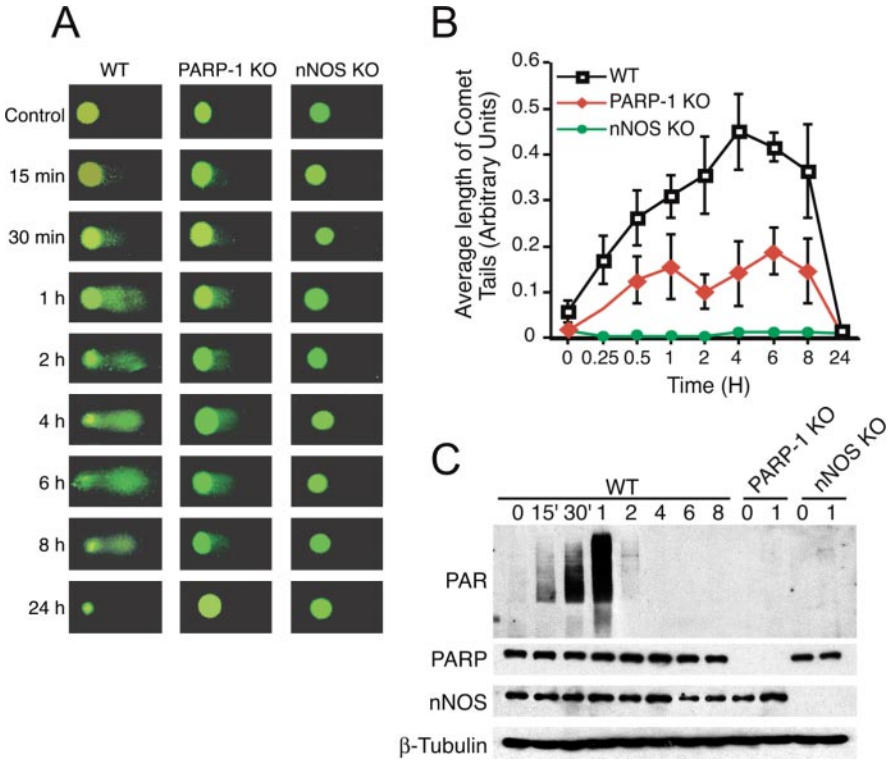

Figure 5. DNA damage is NO dependent and is repaired in PARP-1 KO cortical cultures. Representative confocal images of the comet assay (*A*) and quantitative analysis of the comet assay (*B*) in cortical cultures exposed to NMDA (500 μM). "Tails" can be observed in wild-type (WT) and PARP-1 KO cortical cultures as early as 15 min after NMDA exposure, but tails are not observed in nNOS KO cultures. In wild-type cultures, the tail length continues to extend, and subsequently, at 24 hr only remnants of DNA remain in the dead nucleus. In contrast, in the PARP-1 KO samples, the tail length resolves, and the nuclear morphology is retained. Data are the mean values of three independent experiments ± SD. *C*, PAR polymer formation, a measure of PARP-1 activation, correlates with the time course of DNA damage in wild-type cultures. No PAR formation is observed in the PARP-1 KO cultures, and little PAR polymer is detected in the nNOS KO cultures. Immunoblot confirms that PARP-1 is absent in PARP-1 KO and that nNOS is absent in nNOS KO, respectively. Immunoblot for β-tubulin was used as a loading control. These experiments were repeated at least two times with similar results.

DNA damage and PARP-1 activation is NO dependent

To explore the potential mechanisms by which NMDA receptor stimulation activates PARP-1 and elicits the translocation of AIF, we monitored DNA damage and PARP-1 activation in cortical neurons after NMDA receptor stimulation (Fig. 5). DNA fragmentation was monitored by the comet assay, which detects DNA fragmentation after electrophoresis of cells, and monitoring DNA integrity by SYBR Green staining (Oliver et al., 1999, 2001). Cells with intact DNA have compact circular staining, whereas cells with DNA damage have bright tails that resemble comets. By comet assay, NMDA receptor stimulation elicits DNA damage within 15 min after the insult (Fig. 5*A*). DNA damage continues to increase up to 4 hr after the initial NMDA insult (Fig. 5*A*,*B*) and begins to decrease at ~6–8 hr, probably secondary to the death of neurons (Fig. 4*A*,*B*). Comet tails are completely absent at 24 hr, consistent with the death of cortical neurons (Fig. 5*A*,*B*). In PARP-1 KO cortical cultures, DNA damage also occurs, but tail lengths are shorter (Fig. 5*A*,*B*). The shorter comet tail lengths in PARP-1 KO cultures is probably secondary to the absence of AIF translocation and endonuclease-mediated DNA damage as well as DNA repair processes, which are able to function in PARP-1 KO cultures, because the majority of neurons survive NMDA excitotoxicity. To establish whether NO is involved in DNA damage, comet tail lengths were also examined in cortical neuronal cultures from mice lacking the gene for nNOS (nNOS KO). It has been proposed that NO combines with the superoxide anion to form peroxynitrite to damage DNA, which then activates PARP-1. Cortical neurons from nNOS KO mice have minimal DNA damage at all time points after NMDA administration (Fig. 5*A*,*B*). PARP-1 is activated by DNA strand breaks (de Murcia et al., 1994); therefore, PARP activity was determined by immunoblot detection of poly(ADP-ribose) (PAR) polymer formation with an antibody against the PAR polymer (Fig. 5*C*) (Mandir et al., 2000). PARP-1 activation is observed within 15 min after NMDA receptor stimulation (Fig. 5*C*), coincident with the presence of DNA damage (Fig. 5, compare *A* and *C*). PARP-1 activation is not detected in PARP-1 KO mice, as expected. Although other PARP enzymes have been identified, the immunoblot assay for detecting PARP activation is probably below the limits of detection for these other alternative PARP enzymes. Furthermore, it is not known whether other PARP isoforms are activated by NMDA receptor stimulation. Consistent with the observation that DNA damage does not occur in nNOS KO cortical cultures, we fail to observe any PARP-1 activation in nNOS KO cultures stimulated with NMDA (Fig. 5*C*). These observations suggest that NMDA receptor stimulation causes DNA fragmentation in an nNOS-derived NO-dependent manner, which then activates PARP-1.

AIF translocation mediates NMDA excitotoxicity

To ascertain whether AIF translocation is involved in NMDA excitotoxicity, we monitored the ability of forced overexpression of Bcl-2 to blunt NMDA-induced AIF translocation and cell death (Fig. 6). Bcl-2 is an anti-apoptotic protein that blocks the release of AIF (Susin et al., 1999). HSV amplicon vector-mediated delivery was used for overexpression of Bcl-2. HSV amplicon delivery leads to a >95% infection of neurons, as revealed by β-galactosidase staining of control LacZ-infected neu-

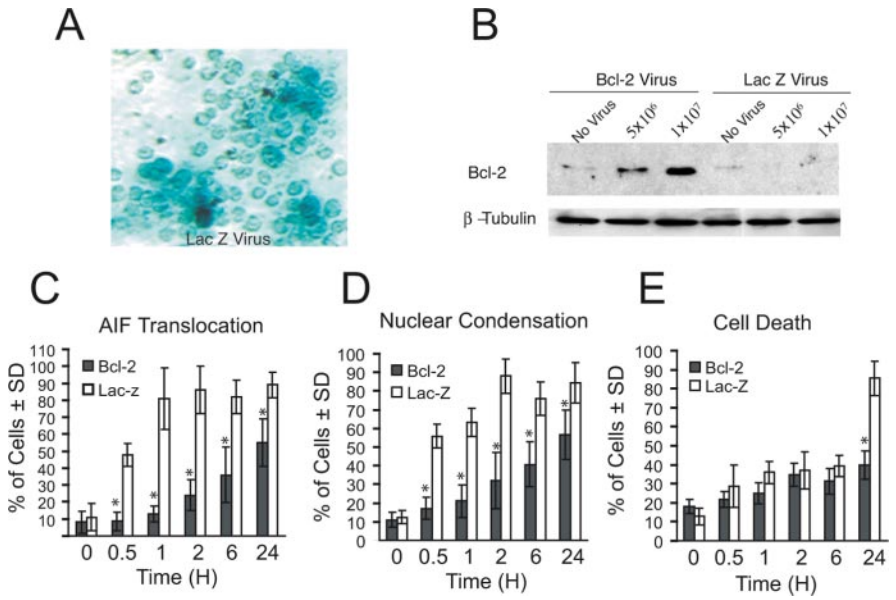

Figure 6. Bcl-2 prevents translocation of AIF and blocks NMDA excitotoxicity. *A*, Herpes simplex viruses show a high infection efficiency in cultured cortical neurons. Viral particles (1×10^7; 100 MOI) of control LacZ-expressing herpes simplex viruses were added to each well (1 ml) of cultured cortical neurons (14 DIV), and after 24 hr, the cultures were stained for β-galactosidase. The picture was taken with a light microscope under a 32× objective lens. *B*, Overexpression of Bcl-2 in neurons. Cultured cortical neurons (in 24-well plates, each well containing 1 ml) were transduced with indicated doses of either Bcl-2-expressing HSVBcl-2 or control β-galactosidase-expressing HSVlacZ herpes simplex viruses. After 24 hr of infection and expression, cells were harvested for Western blotting. These experiments were repeated at least three times with similar results. *C–E*, Bcl-2 retards AIF translocation (*C*) and nuclear condensation (*D*) and partially protects (*E*) in wild-type cortical neurons after exposure to NMDA (500 μM). Cortical cultures were infected with a Bcl-2- or β-galactosidase-expressing herpes simplex virus amplicon vector 24 hr before NMDA treatment. AIF translocation and nuclear shrinkage were observed with confocal microscopy at indicated time points. Bcl-2 provides a partial reduction of AIF translocation, nuclear shrinkage, and cell death. These experiments were repeated at least three times with similar results. Data are the mean values of three independent experiments ± SD. Significance was determined by a one-way ANOVA with Student's *t* test; $^*p \leq 0.05$.

rons (Fig. 6*A*). Overexpression of Bcl-2 in cortical neurons using HSV amplicon vector-mediated transduction was verified by Western blot analysis, which indicates that Bcl-2 is significantly overexpressed compared with LacZ-infected or -noninfected neuronal cultures (Fig. 6*B*). Bcl-2 overexpression dramatically inhibits AIF translocation at 30 min, 1, and 2 hr after NMDA administration and reduces AIF translocation by >50% at 6 hr and 30% at 24 hr (Fig. 6*C*). Nuclear condensation is dramatically reduced at 30 min, 1, and 2 hr after NMDA receptor stimulation. At 6 and at 24 hr, nuclear condensation is reduced by ~35 and 30%, respectively. In another set of cultures, we assessed cell death by cell counting using an objective automated cell-counting system (Gonzalez-Zulueta et al., 1998). Neuronal cell death is only reduced at 24 hr by ~40%, similar to the percentage of cells that fail to translocate AIF after NMDA receptor stimulation (Fig. 6*D*). To confirm that AIF plays a role in NMDA excitotoxicity, cortical neurons were treated with a neutralizing affinity-purified anti-AIF antibody (Yu et al., 2002) before NMDA administration. Western blot analysis indicates that the affinity-purified antibody only recognizes AIF on Western blot (Fig. 7*A*), and previous studies indicate that it is an effective neutralizing antibody (Yu et al., 2002). The neutralizing AIF antibody was administered via the BioPORTER protein delivery reagent. Using this protein delivery system, >95% of the neurons receive AIF antibody, as indicated by the presence of a fluorescent (FITC) marker (Fig. 7*B*), which is coadministered with the antibody. Neurons carrying the neutralizing AIF antibody are resistant to NMDA excitotoxicity, because their nuclei fail to condense after NMDA receptor administration (Fig. 7*C*). Administering an equivalent quantity of rabbit IgG fails to alter NMDA excitotoxicity, and preadsorbing anti-AIF antibody with excess AIF peptides results in failure to block NMDA-induced nuclear condensation (Fig. 7*C*), thus confirming the specificity of the neutralizing antibody. We cannot exclude the possibility that the AIF antibody is interacting with other proteins that we have failed to detect but that nevertheless could be neutralized and account for the neuroprotection. However, the fact that NMDA excitotoxicity and AIF release is PARP-1 dependent, and the time course of PARP-1 activation correlates with AIF translocation coupled with AIF neutralizing antibody experiments, suggest that NMDA receptor excitotoxicity is mediated via the mitochondrial release of AIF and its translocation to the nucleus.

PARP-1-dependent AIF translocation occurs *in vivo* after intrastriatal NMDA injection

To examine whether AIF translocation also occurs *in vivo*, we injected NMDA (66.7 mM in 0.3 μl) into the striatum of either wild-type or PARP-1 KO mice under conditions that induce significant lesions in wild-type mice but no lesion in PARP-1 KO mice (Mandir et al., 2000). Consistent with the *in vitro* cortical neuronal culture results (Fig. 1), the intrastriatal stereotactic microinjection of NMDA induces AIF translocation in a PARP-1-dependent manner *in vivo* (Fig. 8). We examined the striata 6 hr after the NMDA injection, because PARP activity peaks at ~4 hr after NMDA injection (Mandir et al., 2000). Six hours after the NMDA injection, >50% of the neurons from the wild-type mice show AIF translocation to the nucleus, as revealed by confocal immunohistochemistry (Fig. 8*A*,*B*). Most of the cells with AIF translocation are neurons, as indicated by positive staining with the neuron-specific marker NeuN (Koketsu et al., 2003) (Fig. 8*A*). Subcellular fractionation, followed by immunoblotting analysis (Fig. 8*C*), confirms that AIF only translocates to the nucleus in wild-type animals after intrastriatal NMDA injection. Cyt C fails to translocate from the mitochondria to the cytosol at 6 hr in both wild-type and PARP-1 KO mice (Fig. 8*C*). Thus, NMDA excitotoxicity induces AIF release in a PARP-1-dependent manner *in vivo*.

Discussion

The major finding of this paper is that AIF is an important excitotoxic mediator after NMDA receptor stimulation. NMDA excitotoxicity is caspase independent under conditions in which PARP-1 cell-death pathways predominate. NMDA exposure induces AIF translocation, mitochondrial membrane depolarization, and phosphatidyl serine exposure on the cell surface, which appear to precede Cyt C release and caspase-3 activation. Moreover, AIF translocation parallels PARP-1 activation and does not occur in PARP-1 null neurons or in the presence of PARP inhibitors. NMDA excitotoxicity is significantly reduced by a neutral-

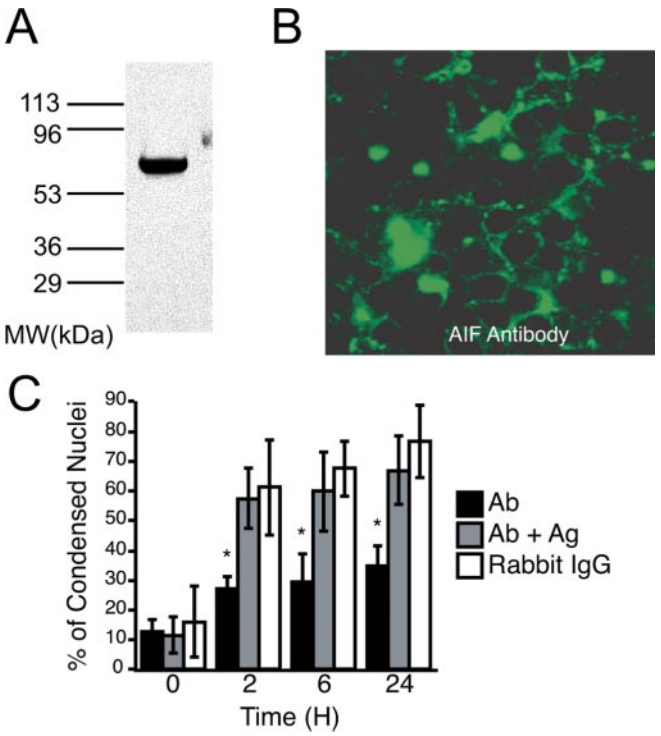

Figure 7. AIF translocation mediates NMDA excitotoxicity *A*, Representative Western blot of AIF antibody in cortical cultures. MW, Molecular weight. *B*, Representative picture of neurons delivered with FITC-conjugated AIF Ab. Cultured neurons (14 DIV) were incubated with the Ab–BioPORTER reagent mixtures for 4 hr and then subjected to confocal microscopy (40× oil objective lens). These experiments were repeated at least three times with similar results. *C*, Cell viability after transduction with BioPORTER protein delivery reagent of anti-AIF antibody, rabbit IgG, or anti-AIF antibody plus the immunogenic peptides (Ab + Ag) (amino acids 151–170 and 181–200) and exposure to NMDA (500 μM). Cortical cultures were fixed, stained with Toto-3, and scanned with a laser confocal microscope. Cells were scored as either dead or alive based on their shapes and nuclear morphology. Data are expressed as the means ± SD. Significance was determined by a one-way ANOVA with Student's *t* test; $^*p < 0.05$.

izing antibody to AIF, and Bcl-2 overexpression reduces AIF translocation and concomitantly reduces NMDA excitotoxicity. These results indicate that NMDA excitotoxicity and the appearance of apoptotic indices of cell death are mediated via AIF in a PARP-1-dependent manner.

Our data suggests that Cyt C is released after AIF translocates to the nucleus. However, we cannot exclude the possibility that Cyt C release is occurring simultaneously with AIF because of the failure to detect Cyt C dissipation via confocal analysis or Cyt C cytosolic translocation via subcellular fractionation analysis. On the other hand, we only observe significant caspase activity at 2 hr after NMDA administration, consistent with our observation that Cyt C release occurs after AIF translocation. Thus, even if our methods for assessing Cyt C release are not sensitive enough to detect a coincident release of Cyt C and AIF translocation, the caspase activation assay suggests that any Cyt C release that may occur coincident with AIF is not sufficient to activate the apoptosome and initiate caspase activation until long after AIF has translocated into the nucleus. We observed a similar time course of AIF translocation versus Cyt C release and caspase activation after PARP-1-dependent cell death in fibroblasts (Yu et al., 2002).

The potentially late release of Cyt C and the late activation of caspases coupled with caspase-independent release of AIF before caspase activation suggests that caspase activation is dispensable in NMDA-mediated neuronal death. Although we cannot rule out a potential role for caspase-2 in this process, the late activation of other caspases would suggest that this is not a primary event in NMDA-mediated AIF-induced cell death. Thus, NMDA receptor-mediated neuronal cell death involves, in part, PARP-1 activation and subsequent AIF translocation, which induces a caspase-independent death program. PARP-1-dependent cell death in fibroblasts after MNNG treatment also involves AIF and exhibits a very similar profile of AIF translocation, mitochondrial depolarization, and phosphatidyl serine exposure that precedes Cyt C release and caspase activation (Yu et al., 2002). Under certain conditions, AIF nuclear translocation requires caspase activation (Arnoult et al., 2002, 2003), but consistent with our results, other death-inducing paradigms involving AIF can occur independent from caspase activation (Daugas et al., 2000; Cregan et al., 2002; Yu et al., 2002). These differences in caspase-dependent and -independent release of AIF are likely attributable to the cellular context and death-inducing stimuli.

Under conditions in which PARP-1-mediated cell-death pathways predominant, AIF appears to kill cells in a caspase-independent manner. Consistent with the notion that AIF can induce neuronal cell death in a caspase-independent manner, adenoviral-mediated overexpression of AIF induces neuronal cell death in a Bax- and caspase-independent manner (Cregan et al., 2002). Other forms of neuronal cell death involve caspase activation, such as p53-induced neuronal injury (Xiang et al., 1996, 1998; Cregan et al., 2002). However, in neurons lacking Apaf-1, AIF is responsible for a delayed-onset caspase-independent cell death (Cregan et al., 2002). Thus, neurons can die under caspase-dependent mechanisms, caspase-independent mechanisms, or both, depending on the insult. After NMDA excitotoxicity, we believe that AIF translocation and subsequent nuclear condensation is one of the irreversible and fatal events. Once it occurs, the neuron is committed to die, because large-scale DNA fragmentation accompanies the nuclear morphological changes. The late activation of caspases after nuclear AIF translocation may facilitate the death process of neurons. Different paradigms of NMDA receptor stimulation can kill neurons, in part through caspase activation (Tenneti et al., 1998). Our paradigm of NMDA receptor stimulation primarily activates NO–PARP-1-dependent cell death pathways, whereas other paradigms activate additional death pathways. The differences are probably attributable to the strength and length of the NMDA receptor stimulus.

Our observations presented here link NMDA receptor-induced excitotoxicity with NO production, DNA damage, PARP-1 activation, and AIF translocation from the mitochondria to the nucleus. In PARP-1 KO neuronal cultures and wild-type cultures treated with PARP inhibitors, AIF translocation is undetectable, indicating that PARP-1 activation is required for AIF translocation. In addition, the results that AMPA receptor-induced excitotoxicity, which kills neurons through a PARP-independent mechanism (Mandir et al., 2000), can trigger Cyt C release but fails to induce significant AIF translocation in both wild-type neurons and PARP-1 null neurons further confirms the importance of PARP activation in AIF translocation. PARP-1 activation is coincident with DNA damage, which is reflected in our sensitive comet and PARP activation assays. Compared with wild-type neurons, DNA fragmentation in PARP-1 KO neurons after NMDA exposure is dramatically reduced. Although there is nNOS activation and NO formation in PARP-1 KO neurons, which causes primary DNA damage, there is no AIF translocation, and accordingly, there is no subsequent secondary DNA damage. Furthermore, the dramatic reduction of comet tail length after the initial

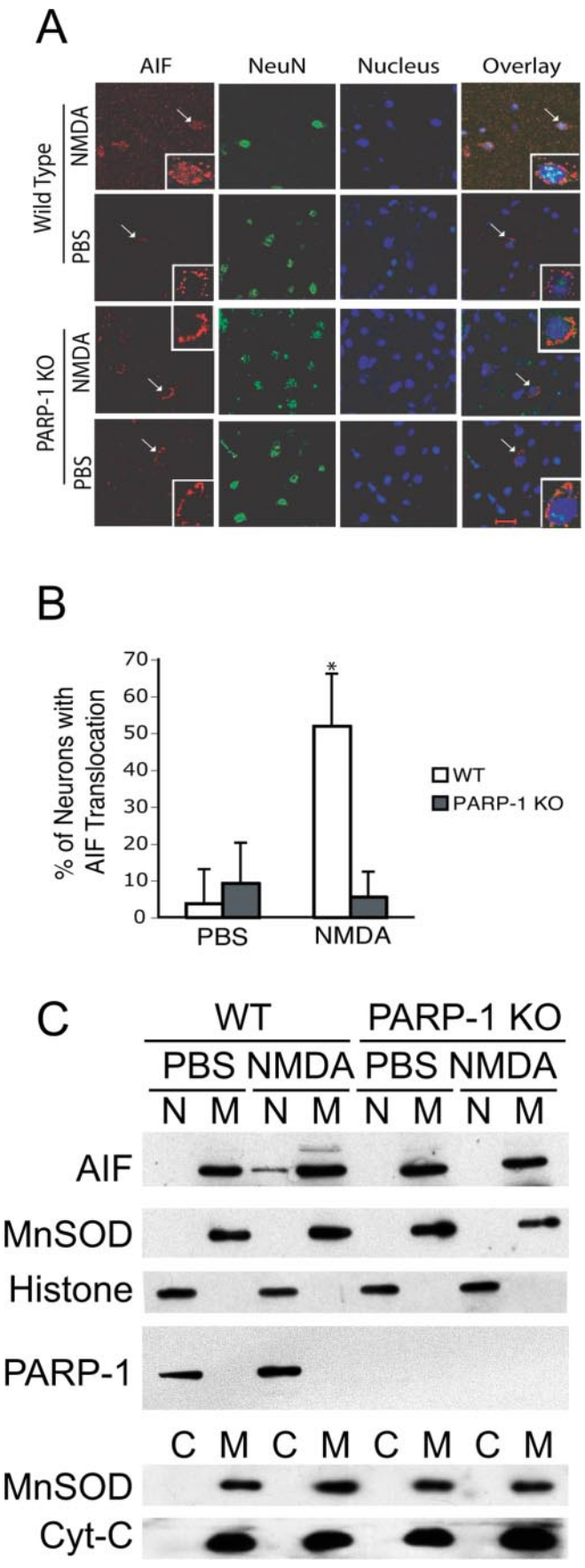

Figure 8. Intrastriatal NMDA injection causes AIF translocation in striatum of wild-type (WT) but not PARP-1 KO mice. *A*, Representative images of immunohistochemical double staining for AIF and neuron-specific marker NeuN. Intrastriatal NMDA injection causes AIF translocation in striatal neurons of wild-type but not PARP-1 KO mice. The white color reflects the colocalization of AIF (red), neuronal marker NeuN (green), and nuclei (blue). Insets, Enlarged pictures of those cells pointed by arrows. Scale bar, 10 μm. *B*, Quantitative analysis of striatal neuronal cells with AIF translocation. *$p < 0.05$ (Student's *t* test). *C*, Western blot analysis of mice striatum after NMDA or vehicle injection. Striatum from wild-type or PARP-1 KO mice 6 hr after NMDA and PBS injection was subjected to fractionation and immunoblotting analysis with anti-AIF antibody. A total of 5 μg of protein was loaded in each lane. Striatum of wild-type mice ipsilateral to NMDA injection shows nuclear translocation of AIF, whereas PBS injection does not cause any injury to the striatum nor AIF translocation. PARP-1 KO mice are resistant to intrastriatal NMDA injection, consistent with the previous results (Mandir et al., 2000), and AIF translocation is not observed in striatum of NMDA- or PBS-injected PARP-1 KO mice. Cyt C is undetectable in the cytosolic fraction (C) by Western blot analysis. MnSOD and histone serve as mitochondrial (M) and nuclear (N) markers, respectively. Immunoblotting with anti-PARP-1 antibody confirms that PARP-1 is absent in PARP-1 KO mice. Three to four WT and PARP-1 KO mice striata were pooled for each fractionation, and similar results were obtained at least three times with three separate pooled striata.

NMDA insult is probably attributable to DNA repair, which occurs independently of PARP-1 in the PARP-1 KO cells (Shieh et al., 1998; Sallmann et al., 2000). Other PARPs, such as PARP-2, appear to compensate for the lack of PARP-1 in the DNA replication process (Schreiber et al., 2002).

After PARP-1 activation, the cell consumes NAD^+ and ATP, leading to the depletion of cellular energy stores and at the same time initiating synthesis of large amounts of PAR polymers (Lautier et al., 1993; de Murcia et al., 1994). Given the fact that neutralizing AIF with an anti-AIF antibody or Bcl-2 overexpression can protect cells from PARP-1-mediated neuronal death, NAD^+ and ATP decrements may not be sufficient to induce neuronal death. NAD^+ and ATP decrements or depletion are also unlikely to trigger AIF translocation. When isolated mitochondria are incubated in a NAD^+-free buffer, we fail to observe release of AIF from mitochondria (S.-W. Yu, V. L. Dawson, T. M. Dawson, unpublished observations). However, recent studies suggest that NAD^+ depletion and mitochondrial permeability transition may be necessary steps linking PARP-1 activation, AIF nuclear translocation, and cell death (Alano et al., 2004). Thus, NAD^+ depletion may be necessary, but not sufficient, for PARP-1-dependent AIF nuclear translocation and cell death. The exact roles of NAD^+ and ATP decrements and/or depletion in AIF release from the mitochondria and translocation to the nucleus require additional study, but other mechanisms secondary to PARP-1 activation may also play key roles in the release of AIF.

In a manner similar to Cyt C, AIF is a mitochondrial-associated protein that appears to play dual but separable functions in the cell (Susin et al., 1999; Miramar et al., 2001; Klein et al., 2002). Under normal physiological circumstances, AIF is associated with mitochondria and seems to function as an antioxidant (Miramar et al., 2001; Klein et al., 2002). However, when AIF is released from the mitochondria, it translocates to the nucleus to induce nuclear condensation and cell death. Our observations indicate that the death-inducing effect of AIF is mediated via its translocation. Because downregulation of AIF in the Harlequin mouse leads to the degeneration of cerebellar and retinal neurons (Klein et al., 2002), it will be important to block AIF translocation from the mitochondria to the nucleus without impairing its important physiological functions in the mitochondria when developing strategies to block excitotoxicity.

References

Affar EB, Duriez PJ, Shah RG, Sallmann FR, Bourassa S, Kupper JH, Burkle A, Poirier GG (1998) Immunodot blot method for the detection of poly(ADP-ribose) synthesized in vitro and in vivo. Anal Biochem 259:280–283.

Affar EB, Duriez PJ, Shah RG, Winstall E, Germain M, Boucher C, Bourassa S, Kirkland JB, Poirier GG (1999) Immunological determination and size characterization of poly(ADP-ribose) synthesized in vitro and in vivo. Biochim Biophys Acta 1428:137–146.

Alano CC, Ying W, Swanson RA (2004) Poly(ADP-ribose) polymerase-1-mediated cell death in astrocytes requires NAD+ depletion and mitochondrial permeability transition. J Biol Chem 279:18895–18902.

Arnoult D, Parone P, Martinou JC, Antonsson B, Estaquier J, Ameisen JC (2002) Mitochondrial release of apoptosis-inducing factor occurs downstream of cytochrome c release in response to several proapoptotic stimuli. J Cell Biol 159:923–929.

Arnoult D, Gaume B, Karbowski M, Sharpe JC, Cecconi F, Youle RJ (2003) Mitochondrial release of AIF and EndoG requires caspase activation downstream of Bax/Bak-mediated permeabilization. EMBO J 22:4385–4399.

Ayata C, Ayata G, Hara H, Matthews RT, Beal MF, Ferrante RJ, Endres M, Kim A, Christie RH, Waeber C, Huang PL, Hyman BT, Moskowitz MA (1997) Mechanisms of reduced striatal NMDA excitotoxicity in type I nitric oxide synthase knock-out mice. J Neurosci 17:6908–6917.

Bowers WJ, Howard DF, Brooks AI, Halterman MW, Federoff HJ (2001) Expression of vhs and VP16 during HSV-1 helper virus-free amplicon packaging enhances titers. Gene Ther 8:111–120.

Burkart V, Wang ZQ, Radons J, Heller B, Herceg Z, Stingl L, Wagner EF, Kolb H (1999) Mice lacking the poly(ADP-ribose) polymerase gene are resistant to pancreatic beta-cell destruction and diabetes development induced by streptozocin. Nat Med 5:314–319.

Cregan SP, Fortin A, MacLaurin JG, Callaghan SM, Cecconi F, Yu SW, Dawson TM, Dawson VL, Park DS, Kroemer G, Slack RS (2002) Apoptosis-inducing factor is involved in the regulation of caspase-independent neuronal cell death. J Cell Biol 158:507–517.

Daugas E, Susin SA, Zamzami N, Ferri KF, Irinopoulou T, Larochette N, Prevost MC, Leber B, Andrews D, Penninger J, Kroemer G (2000) Mitochondrio-nuclear translocation of AIF in apoptosis and necrosis. Faseb J 14:729–739.

Dawson VL, Dawson TM (1998) Nitric oxide in neurodegeneration. Prog Brain Res 118:215–229.

de Murcia G, Schreiber V, Molinete M, Saulier B, Poch O, Masson M, Niedergang C, Menissier de Murcia J (1994) Structure and function of poly(ADP-ribose) polymerase. Mol Cell Biochem 138:15–24.

Du L, Zhang X, Han YY, Burke NA, Kochanek PM, Watkins SC, Graham SH, Carcillo JA, Szabo C, Clark RS (2003) Intra-mitochondrial poly(ADP-ribosylation) contributes to NAD+ depletion and cell death induced by oxidative stress. J Biol Chem 278:18426–18433.

Eliasson MJ, Sampei K, Mandir AS, Hurn PD, Traystman RJ, Bao J, Pieper A, Wang ZQ, Dawson TM, Snyder SH, Dawson VL (1997) Poly(ADP-ribose) polymerase gene disruption renders mice resistant to cerebral ischemia. Nat Med 3:1089–1095.

Endres M, Wang ZQ, Namura S, Waeber C, Moskowitz MA (1997) Ischemic brain injury is mediated by the activation of poly(ADP-ribose) polymerase. J Cereb Blood Flow Metab 17:1143–1151.

Ferrer I, Planas AM (2003) Signaling of cell death and cell survival following focal cerebral ischemia: life and death struggle in the penumbra. J Neuropathol Exp Neurol 62:329–339.

Gonzalez-Zulueta M, Ensz LM, Mukhina G, Lebovitz RM, Zwacka RM, Engelhardt JF, Oberley LW, Dawson VL, Dawson TM (1998) Manganese superoxide dismutase protects nNOS neurons from NMDA and nitric oxide-mediated neurotoxicity. J Neurosci 18:2040–2055.

Ha HC, Snyder SH (1999) Poly(ADP-ribose) polymerase is a mediator of necrotic cell death by ATP depletion. Proc Natl Acad Sci USA 96:13978–13982.

Huang Z, Huang PL, Panahian N, Dalkara T, Fishman MC, Moskowitz MA (1994) Effects of cerebral ischemia in mice deficient in neuronal nitric oxide synthase. Science 265:1883–1885.

Klein JA, Longo-Guess CM, Rossmann MP, Seburn KL, Hurd RE, Frankel WN, Bronson RT, Ackerman SL (2002) The harlequin mouse mutation downregulates apoptosis-inducing factor. Nature 419:367–374.

Koketsu D, Mikami A, Miyamoto Y, Hisatsune T (2003) Nonrenewal of neurons in the cerebral neocortex of adult macaque monkeys. J Neurosci 23:937–942.

Koppenol WH, Moreno JJ, Pryor WA, Ischiropoulos H, Beckman JS (1992) Peroxynitrite, a cloaked oxidant formed by nitric oxide and superoxide. Chem Res Toxicol 5:834–842.

Lautier D, Lagueux J, Thibodeau J, Menard L, Poirier GG (1993) Molecular and biochemical features of poly (ADP-ribose) metabolism. Mol Cell Biochem 122:171–193.

Lynch DR, Guttmann RP (2002) Excitotoxicity: perspectives based on *N*-methyl-D-aspartate receptor subtypes. J Pharmacol Exp Ther 300:717–723.

Mandir AS, Przedborski S, Jackson-Lewis V, Wang ZQ, Simbulan-Rosenthal CM, Smulson ME, Hoffman BE, Guastella DB, Dawson VL, Dawson TM (1999) Poly(ADP-ribose) polymerase activation mediates 1-methyl-4-phenyl-1, 2,3,6-tetrahydropyridine (MPTP)-induced parkinsonism. Proc Natl Acad Sci USA 96:5774–5779.

Mandir AS, Poitras MF, Berliner AR, Herring WJ, Guastella DB, Feldman A, Poirier GG, Wang ZQ, Dawson TM, Dawson VL (2000) NMDA but not non-NMDA excitotoxicity is mediated by Poly(ADP-ribose) polymerase. J Neurosci 20:8005–8011.

Masutani M, Suzuki H, Kamada N, Watanabe M, Ueda O, Nozaki T, Jishage K, Watanabe T, Sugimoto T, Nakagama H, Ochiya T, Sugimura T (1999) Poly(ADP-ribose) polymerase gene disruption conferred mice resistant to streptozotocin-induced diabetes. Proc Natl Acad Sci USA 96:2301–2304.

Miller TM, Moulder KL, Knudson CM, Creedon DJ, Deshmukh M, Korsmeyer SJ, Johnson Jr EM (1997) Bax deletion further orders the cell death pathway in cerebellar granule cells and suggests a caspase-independent pathway to cell death. J Cell Biol 139:205–217.

Miramar MD, Costantini P, Ravagnan L, Saraiva LM, Haouzi D, Brothers G, Penninger JM, Peleato ML, Kroemer G, Susin SA (2001) NADH oxidase activity of mitochondrial apoptosis-inducing factor. J Biol Chem 276:16391–16398.

Olive PL, Durand RE, Banath JP, Johnston PJ (2001) Analysis of DNA damage in individual cells. Methods Cell Biol 64:235–249.

Oliver FJ, Menissier-de Murcia J, Nacci C, Decker P, Andriantsitohaina R, Muller S, de la Rubia G, Stoclet JC, de Murcia G (1999) Resistance to endotoxic shock as a consequence of defective NF-kappaB activation in poly (ADP-ribose) polymerase-1 deficient mice. EMBO J 18:4446–4454.

Panahian N, Yoshida T, Huang PL, Hedley-Whyte ET, Dalkara T, Fishman MC, Moskowitz MA (1996) Attenuated hippocampal damage after global cerebral ischemia in mice mutant in neuronal nitric oxide synthase. Neuroscience 72:343–354.

Pieper AA, Verma A, Zhang J, Snyder SH (1999) Poly (ADP-ribose) polymerase, nitric oxide and cell death. Trends Pharmacol Sci 20:171–181.

Pieper AA, Walles T, Wei G, Clements EE, Verma A, Snyder SH, Zweier JL (2000) Myocardial postischemic injury is reduced by polyADPripose polymerase-1 gene disruption. Mol Med 6:271–282.

Przedborski S, Jackson-Lewis V, Yokoyama R, Shibata T, Dawson VL, Dawson TM (1996) Role of neuronal nitric oxide in 1-methyl-4-phenyl-1,2,3,6-tetrahydropyridine (MPTP)-induced dopaminergic neurotoxicity. Proc Natl Acad Sci USA 93:4565–4571.

Sallmann FR, Vodenicharov MD, Wang ZQ, Poirier GG (2000) Characterization of sPARP-1. An alternative product of PARP-1 gene with poly(ADP-ribose) polymerase activity independent of DNA strand breaks. J Biol Chem 275:15504–15511.

Samdani AF, Dawson TM, Dawson VL (1997) Nitric oxide synthase in models of focal ischemia. Stroke 28:1283–1288.

Sattler R, Tymianski M (2001) Molecular mechanisms of glutamate receptor-mediated excitotoxic neuronal cell death. Mol Neurobiol 24:107–129.

Schreiber V, Ame JC, Dolle P, Schultz I, Rinaldi B, Fraulob V, Menissier-de Murcia J, de Murcia G (2002) Poly(ADP-ribose) polymerase-2 (PARP-2) is required for efficient base excision DNA repair in association with PARP-1 and XRCC1. J Biol Chem 277:23028–23036.

Shieh WM, Ame JC, Wilson MV, Wang ZQ, Koh DW, Jacobson MK, Jacobson EL (1998) Poly(ADP-ribose) polymerase null mouse cells synthesize ADP-ribose polymers. J Biol Chem 273:30069–30072.

Susin SA, Lorenzo HK, Zamzami N, Marzo I, Snow BE, Brothers GM, Mangion J, Jacotot E, Costantini P, Loeffler M, Larochette N, Goodlett DR,

Aebersold R, Siderovski DP, Penninger JM, Kroemer G (1999) Molecular characterization of mitochondrial apoptosis-inducing factor. Nature 397:441–446.

Szabo C, Dawson VL (1998) Role of poly(ADP-ribose) synthetase in inflammation and ischaemia-reperfusion. Trends Pharmacol Sci 19:287–298.

Tenneti L, D'Emilia DM, Troy CM, Lipton SA (1998) Role of caspases in *N*-methyl-D-aspartate-induced apoptosis in cerebrocortical neurons. J Neurochem 71:946–959.

Xiang H, Hochman DW, Saya H, Fujiwara T, Schwartzkroin PA, Morrison RS (1996) Evidence for p53-mediated modulation of neuronal viability. J Neurosci 16:6753–6765.

Xiang H, Kinoshita Y, Knudson CM, Korsmeyer SJ, Schwartzkroin PA, Morrison RS (1998) Bax involvement in p53-mediated neuronal cell death. J Neurosci 18:1363–1373.

Yu SW, Wang H, Poitras MF, Coombs C, Bowers WJ, Federoff HJ, Poirier GG, Dawson TM, Dawson VL (2002) Mediation of poly(ADP-ribose) polymerase-1-dependent cell death by apoptosis-inducing factor. Science 297:259–263.

Zhang J, Dawson VL, Dawson TM, Snyder SH (1994) Nitric oxide activation of poly(ADP-ribose) synthetase in neurotoxicity. Science 263:687–689.

Zhu C, Qiu L, Wang X, Hallin U, Cande C, Kroemer G, Hagberg H, Blomgren K (2003) Involvement of apoptosis-inducing factor in neuronal death after hypoxia-ischemia in the neonatal rat brain. J Neurochem 86:306–317.